Estimation of Regional Surface Layer Wind Field Characteristics Using a Three-Layer Mesoscale Model

Dietrich Heimann

DFVLR-Institute for Atmospheric Physics, Weßling-Oberpfaffenhofen, F.R. Germany

(Manuscript received 07.05.1986, in revised form 31.07.1986)

Abstract:

A hydrostatic three-layer mesoscale model is used to determine the annual frequency distribution of the surface layer winds over the whole area of the orographically structured mesoscale-β region around Frankfurt (Main-Taunus region, 68 × 68 km^2). The model was run, simulating the variation of stability over the course of a typical day for each of the twelve 30° sectors of the geostrophic wind. For each sector the corresponding annual mean value of the geostrophic wind speed was taken. The calculated wind fields were extracted hourly and weighted by the frequency of occurrence of the corresponding geostrophic wind sector, for later utilization.

This procedure enables wind roses to be constructed for all grid squares, and the localization of channeling regimes and diurnal wind systems. The synthetic wind roses are compared with observations and agree well.

Zusammenfassung: Abschätzung regionaler Charakteristika des bodennahen Windfelds mit einem mesoskaligen Dreischichten-Modell

Mit Hilfe eines hydrostatischen Dreischichten-Modells wird die Jahresverteilung der Häufigkeit des bodennahen Windes über dem topographisch gegliederten, mesoskaligen Gebiet um Frankfurt (Main-Taunus-Region, 68 × 68 km^2) flächendeckend bestimmt. Zu diesem Zweck wurden zwölf Modelläufe über jeweils einen typischen Tagesgang für alle 30° Sektoren des geostrophischen Windes durchgeführt, wobei für jeden Sektor die jeweils mittlere jährliche geostrophische Windgeschwindigkeit verwendet wurde. Zur weiteren Auswertung wurden die berechneten Windfelder stündlich ausgelagert und mit der Häufigkeit des dazugehörenden geostrophischen Windes gewichtet.

Auf diese Weise ist es möglich Windrosenfelder zu konstruieren und Einflußbereiche der Leitwirkung und tagesperiodischer Windsysteme zu ermitteln. Die berechneten Windrosen zeigen eine gute Übereinstimmung mit Beobachtungen.

Résumé: Estimation des caractéristiques régionales du champ de vent dans la couche de surface à l'aide d'un modèle d'échelle mésométéorologique à trois couches.

On utilise un modèle hydrostatique d'échelle mésométéorologique afin de déterminer le spectre annuel des fréquences du vent dans la couche de surface sur toute la région aux alentours de Francfort où l'orographie présente une structure d'échelle mésométéorologique de type β (Région de Taunus, 68 × 68 km^2). On a fait en sorte que le modèle simule la variation de stabilité au cours d'une journée typique pour chacun des douze secteurs de 30° du vent géostrophique. On a utilisé pour chaque secteur la moyenne annuelle de la vitesse du vent géostrophique correspondant.

Les champs de vent calculés sont extraits d'heure en heure et pondérés par la fréquence d'occurence du vent géostrophique dans le secteur envisagé pour utilisation ultérieure.

Cette procédure permet la construction de roses des vents pour tous les carrés de la grille, la localisation des régimes où le vent est canalisé et la localisation des systèmes de vent à caractère diurne. Les roses des vents sont comparées aux observations avec lesquelles elles s'accordent bien.

0005-8173/86/04 0518–20 $ 03.00/0

List of Symbols

c_p	specific heat capacity ($c_p = 1005\ J\ kg^{-1}\ K^{-1}$)
C	turbulent transfer coefficient
D	horizontal diffusion
Δt	time step
$\Delta x, \Delta y$	horizontal grid spacing
Δz	thickness of a layer
f	Coriolis parameter ($f = 0.0001\ s^{-1}$)
F	vertical turbulent flux
g	gravity acceleration ($g = 9.81\ m\ s^{-2}$)
γ	vertical gradient of potential temperature
h	height of a surface or interface
k	Karman constant ($k = 0.4$)
k_l	adiabatic exponent ($k_l = 0.28$)
K	diffusion coefficient
ω	vertical velocity relative to an inclined surface
p	pressure
π	Exner function
Pr	Prandtl number
Ri	Richardson number
ρ	density
t	time
T	temperature
θ	potential temperature
V	horizontal wind vector
u, v	horizontal wind components
w	cartesian vertical velocity
u_*	friction velocity
z	height
z_0	roughness length

Bold symbols are horizontal (x- and y-direction) vectors!

List of Subscripts

sub	ground level	g	geostrophic
s	s-layer or upper surface of s-layer	h	horizontal
m	m-layer or upper surface of m-layer	M	momentum
t	t-layer or upper surface of t-layer	H	heat
q	atmospheric boundary layer (s- and m-layer)	adv	advection
x, y	x- or y-components	ent	entrainment

1 Introduction

Many problems of environmental planning and air pollution assessment, like source-receptor relations or pollution impact studies, require the knowledge of the regional wind climatology. It is normally derived from the recordings of nearby weather stations. Where the topography is complex these stations are representative only of a limited area, and are unsuitable for deducing wind field characteristics over the whole of the region.

As WIPPERMANN and GROSS (1981) already showed, a mesoscale model can be a useful substitute for the statistics of measured wind, if the frequency distribution of the large scale geostrophic wind is known. They constructed a wind rose for Mannheim from stationary solutions of the two-dimensional version of the non-hydrostatic FITNAH mesoscale model (GROSS, 1985). The simulations were restricted to cases with stable stratification and to those directions of the geostrophic wind which are not perpendicular to the two-dimensional cross section. The observed wind rose (for stable situations) compares well with the numerically deduced one, and demonstrates the validity of the method.

However, to benefit from synthetic wind statistics one must usually

- consider all sectors of the large scale wind,
- take into account a wide range of stability,
- also consider time-dependent phenomena (e.g. thermal circulations, low level jets).

This, of course, requires a fairly large number of simulated cases. Moreover, two-dimensional models are insufficient for most of the applications. Three-dimensional, and particulary non-hydrostatic models certainly need rather a lot of computer time and storage. This makes them unwieldy, at least for statistical studies. As a suitable compromise a hydrostatic three-layer model was developed for regions with gentle orography which extend horizontally between 50 and 200 km (mesoscale-β) resolved by grid sizes between 2 and 10 km. The hydrostatic approximation is justified as long as the vertical accelerations are by one order of magnitude smaller than the horizontal accelerations. Therefore the inclination of the terrain should not exceed the ratio 1 : 10. It will be shown that this model is handy enough to allow the generation of an adequate number of cases to represent an annual climate even on small computers. However, higher resolutions and steep orography require the use of an advanced non-hydrostatic model.

2 The Model

2.1 Geometrical Structure

The model used in this study belongs to the family of simple mesoscale models. One of the early developments of such models has been introduced by LAVOIE (1972). He applied a one-layer model of the mixing-layer to such complex phenomena as lake-effect storms. KEYSER and ANTHES (1977) improved LAVOIE's model by introducing entrainment processes at the top of the mixing layer, and by utilizing a drag coefficient depending on both the surface heat flux and roughness. Also, HAN, UEYOSHI and DEARDORFF (1982) used a simple one-layer model for their numerical experiments on terrain-induced mesoscale motion. DEADORFF, UEYOSHI and HAN (1984) extended the one layer formulation of the mixed layer by three overlaying model layers defined in a hydrostatic pressure coordinate system. This model was used to study various effects of horizontal inhomogeneities.

The model presented here was developed especially for regional air pollution studies over complex terrain. In the following it will be referred to as REWIMET. The requirements of air pollution modeling have led to a three-layer vertical resolution of a cloud-free model atmosphere, distinguishing a surface

layer, a mixed layer, and a reservoir layer. This scheme is similar to the one used by VAN EGMOND and KESSEBOOM (1983) for dispersion calculations based on wind fields diagnostically derived from measurements. While they assume that the vertical structure is time-dependent but constant throughout the model domain, in REWIMET the heights of the layers can also vary spatially due to the actual mesoscale meteorological situation. The vertical structure of REWIMET is described as follows and illustrated in Figure 1.

1. The model atmosphere extends from the ground h_{sur} up to a level h_t which coincides with a large scale inversion or discontinuity of the vertical temperature profile. This level is represented by a free material surface in the model which is allowed to vary in time and space. This is in contrast to the model formulation of KEYSER and ANTHES (1977) who used a constant model lid but consequently renounced any dynamic process above the boundary layer.
2. The turbulent atmospheric boundary layer (ABL) is assumed to extend from the ground h_{sur} up to a height $h_m \leqslant h_t$ which can be changed by advection and entrainment. The ABL is represented by two sublayers. The lower surface layer (s-layer) between h_{sur} and h_s is defined to follow the terrain with a constant thickness of $\Delta z_s = h_s - h_{sur} = 50$ m. The upper 'mixed' layer (m-layer) reaches from h_s to h_m and is variable in time and space. Turbulent fluxes are considered at the ground and the interface between the two sublayers of the ABL.
3. The third layer (t-layer) is situated above the turbulent ABL between h_m and h_t. The ABL is allowed to grow up to the large scale inversion, i.e. up to h_t in the model. Since the entrainment rate is damped if h_m comes close to h_t, the t-layer cannot completely disappear. It remains as a shallow layer of a few meters in such a case.

In order to permit a wide range of applications the model is time-dependent and designed to treat unstable as well as stable stratifications. In the case of an unstable ABL, the entrainment equation provides for the growth of the m-layer. Air and its properties (momentum, heat, and concentration) are then entrained from the t-layer into the m-layer. After a transition from unstable to stable stratification, the turbulence decays and will occur only within a shallow layer near the ground. Therefore the entrainment equation causes the m-layer to shrink rapidly. During this process air and its properties are now entrained from the m-layer into the overlaying t-layer. The latter then acts as a reservoir for these properties before a renewed growth of the ABL entrains them back into the m-layer. The changes of stability are governed by a prescribed temporal variation of the surface potential temperature θ_{sur}.

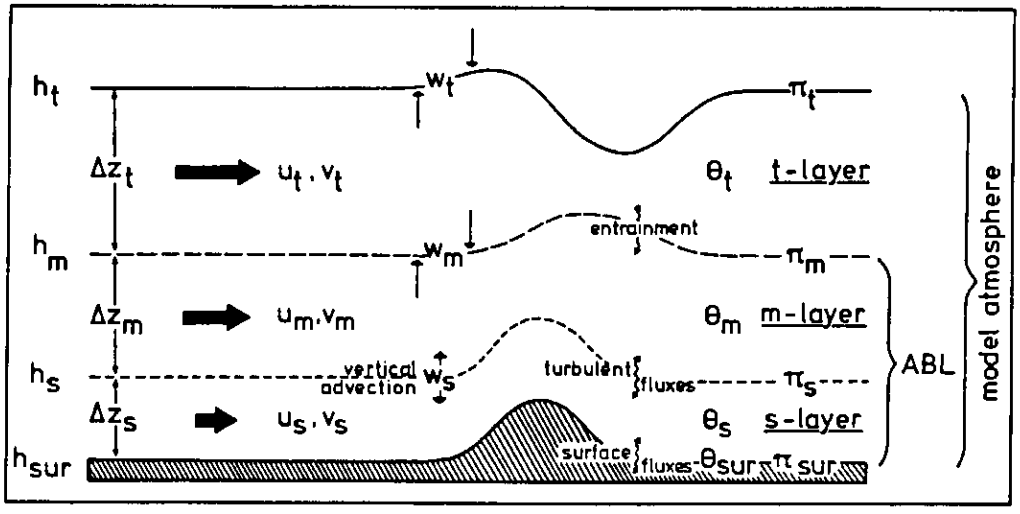

● **Figure 1**
Schematic illustration of the vertical model structure

2.2 The Equations

The model is based on the equations of a hydrostatic, non-divergent, dry atmosphere with a supra-scale forcing and friction due to sub-scale turbulence:

$$\frac{\partial \mathbf{V}}{\partial t} = -\mathbf{V}\cdot\nabla\mathbf{V} - w\frac{\partial \mathbf{V}}{\partial z} + f\mathbf{k}\times(\mathbf{V}_g - \mathbf{V}) - c_p\theta\,\nabla\pi + \mathbf{D}_M - \frac{\partial}{\partial z}\mathbf{F}_M \tag{1}$$

$$\frac{\partial \theta}{\partial t} = -\mathbf{V}\cdot\nabla\theta - w\frac{\partial \theta}{\partial z} + D_H - \frac{\partial}{\partial z}F_H \tag{2}$$

$$\frac{\partial \pi}{\partial t} = -\frac{g}{c_p\theta} \tag{3}$$

$$\frac{\partial w}{\partial z} = -\nabla\cdot\mathbf{V} \tag{4}$$

with

$\pi = \left(\frac{p}{p_0}\right)^{k_l}$ (Exner function); $p_0 = 10^5$ Pa

$\theta = \frac{T}{\pi}$ (potential temperature)

p and π represent the mesoscale variation of the pressure. The superimposed supra-scale pressure gradient is expressed by the geostrophic wind $\mathbf{V}_g$ which has to be prescribed uniformly within the model volume.

A prognostic equation for the concentration of an air pollutant is optional but is not considered within this paper.

The Equations (1) through (4) have to be adapted to the specific attributes of each of the model layers. The following points must be taken into account:

1. The interfaces of the model layers are not horizontal, but depend on x and y.
2. With the exception of the s-layer, the thicknesses of the model layers are not uniform.
3. The levels h_m and h_t are time-dependent.
4. h_{sur} and h_t are material surfaces. No advective fluxes are allowed to permeate them.
5. The interface between s- and m-layer, h_s, is defined to be permeable for both advective and turbulent fluxes. The top of the ABL, h_m, is permeable only in case of entrainment.

The Exner function π and the vertical velocity w are evaluated on the interfaces (h_{sur}, h_s, etc.), whereas the horizontal velocity components u, v, and the potential temperature θ are considered to be vertically uniform within each layer (s-layer, m-layer, t-layer).

As a consequence also the temporal derivatives of u, v, and θ are independent of height within each model layer. Thus, by applying Equations (1) and (2) to the model layers only the vertical advection terms and the pressure gradient term have to be treated specially. A detailed description of the adaptation to the geometrical model structure is given by HEIMANN (1985).

The vertical velocity relative to the inclined interface between the s-layer and the m-layer, ω_s, is related to the cartesian vertical velocity $w_s = w(z \to h_s, z < h_s)$ by

$$\omega_s = w_s - u_s\frac{\partial h_s}{\partial x} - v_s\frac{\partial h_s}{\partial y}$$

ω_s is a measure of the local transport of mass through the interface h_s. Depending on the sign of ω_s the vertical advection contributes either to the m-layer ($\omega_s > 0$) or to the s-layer ($\omega_s < 0$).

The adaptation of the mesoscale pressure gradient term in Equation (1) to the bulk of a model layer requires some modifications. The horizontal gradient of π can be evaluated only on the top (or bottom) surface of a layer. If this surface is not horizontal, compensation must be made for the hydrostatic pressure effect of the slope. Additionally, the vertical change of the pressure gradient within a layer can be expressed by the horizontal gradient of the potential temperature, which by definition does not depend on the height in the layer. In its final form the vertically averaged mesoscale pressure gradient term of a layer can be written as

$$- c_p\, \theta_k\, \nabla\pi_k - g\nabla h_k + \frac{g\,\Delta z_k}{2\theta}\,\nabla\theta_k$$

where k is the subscript denoting the layer or the overlaying surface, i.e. $k \equiv (s, m, t)$. Since the model layers differ from each other with respect to their attributes, the equations have to be formulated separately for each layer.

– equations of the s-layer:

upper surface: $h_s(x, y)$ permeable for advective and turbulent fluxes
thickness: $\Delta z_s = \text{const} = 50$ m
lower surface: $h_{sur}(x, y)$ impermeable

$$\frac{\partial u_s}{\partial t} = - u_s \frac{\partial u_s}{\partial x} - v_s \frac{\partial u_s}{\partial y} - \omega_s \frac{u_2 - u_s}{\Delta z_s} - f(v_g - v_s) -$$
$$- c_p\, \theta_s \frac{\partial \pi_s}{\partial x} - g \frac{\partial h_s}{\partial x} + \frac{g \Delta z_s}{2\theta_s} \frac{\partial \theta_s}{\partial x} + D_{Msx} - \frac{F_{Mxs} - F_{Mxsur}}{\Delta z_s}$$

$$\frac{\partial v_s}{\partial t} = - u_s \frac{\partial v_s}{\partial x} - v_s \frac{\partial v_s}{\partial y} - \omega_s \frac{v_2 - v_s}{\Delta z_s} + f(u_g - u_s) -$$
$$- c_p\, \theta_s \frac{\partial \pi_s}{\partial y} - g \frac{\partial h_s}{\partial y} + \frac{g\,\Delta z_s}{2\theta_s} \frac{\partial \theta_s}{\partial y} + D_{Msy} - \frac{F_{Mys} - F_{Mysur}}{\Delta z_s}$$

$$\frac{\partial \theta_s}{\partial t} = - u_s \frac{\partial \theta_s}{\partial x} - v_s \frac{\partial \theta_s}{\partial y} - \omega_s \frac{\theta_2 - \theta_s}{\Delta z_s} + D_{Hs} - \frac{F_{Hs} - F_{Hsur}}{\Delta z_s}$$

$$\pi_{sur} = \pi_s + \frac{g}{c_p\, \theta_s} \Delta z_s$$

$$\omega_s = - \Delta z_s \left(\frac{\partial u_s}{\partial x} + \frac{\partial v_s}{\partial y} \right)$$

with

$$\left.\begin{array}{l} u_2 = u_s \\ v_2 = v_s \\ \theta_2 = \theta_s \end{array}\right\} \text{ for } \omega_s \geqslant 0; \qquad \left.\begin{array}{l} u_2 = u_m \\ v_2 = v_m \\ \theta_2 = \theta_m \end{array}\right\} \text{ for } \omega_s < 0$$

$$D_{Msx} = K_h \left(\frac{\partial^2 u_s}{\partial x^2} + \frac{\partial^2 u_s}{\partial y^2} \right); \quad D_{Msy} = K_h \left(\frac{\partial^2 v_s}{\partial x^2} + \frac{\partial^2 v_s}{\partial y^2} \right); \quad D_{Hs} = K_h \left(\frac{\partial^2 \theta_s}{\partial x^2} + \frac{\partial^2 \theta_s}{\partial y^2} \right)$$

– equations of the m-layer:

upper surface: $h_m(x, y, t)$ permeable for entrainment fluxes only
thickness: $\Delta z_m(x, y, t) \geqslant 50$ m
lower surface: $h_s(x, y)$ permeable for advective and turbulent fluxes

$$\frac{\partial u_m}{\partial t} = -u_m \frac{\partial u_m}{\partial x} - v_m \frac{\partial u_m}{\partial y} - \omega_s \frac{u_m - u_1}{\Delta z_m} - f(v_g - v_m) - c_p \theta_m \frac{\partial \pi_m}{\partial x} - g \frac{\partial h_m}{\partial x} + \frac{g \Delta z_m}{2\theta_m} \frac{\partial \theta_m}{\partial x} + D_{Mmx} + \frac{F_{Mxs}}{\Delta z_m} + \left.\frac{\partial u_m}{\partial t}\right|_{ent}$$

$$\frac{\partial v_m}{\partial t} = -u_m \frac{\partial v_m}{\partial x} - v_m \frac{\partial v_m}{\partial y} - \omega_s \frac{v_m - v_1}{\Delta z_m} + f(u_g - u_m) - c_p \theta_m \frac{\partial \pi_m}{\partial y} - g \frac{\partial h_m}{\partial y} + \frac{g \Delta z_m}{2\theta_m} \frac{\partial \theta_m}{\partial y} + D_{Mmy} + \frac{F_{Mys}}{\Delta z_m} + \left.\frac{\partial v_m}{\partial t}\right|_{ent}$$

$$\frac{\partial \theta_m}{\partial t} = -u_m \frac{\partial \theta_m}{\partial x} - v_m \frac{\partial \theta_m}{\partial y} - \omega_s \frac{\theta_1 - \theta_m}{\Delta z_m} + D_{Hm} + \frac{F_{Hs}}{\Delta z_m} + \left.\frac{\partial \theta_m}{\partial t}\right|_{ent}$$

$$\pi_s = \pi_m + \frac{g}{c_p \theta_m} \Delta z_m$$

$$\frac{\partial h_m}{\partial t} = \left.\frac{\partial h_m}{\partial t}\right|_{adv} + \left.\frac{\partial h_m}{\partial t}\right|_{ent} = \omega_s - \left(\frac{\partial (u_m \Delta z_m)}{\partial x} + \frac{\partial (v_m \Delta z_m)}{\partial y} \right) + \left.\frac{\partial h_m}{\partial t}\right|_{ent}$$

with

$$\left.\begin{aligned} u_1 &= u_s \\ v_1 &= v_s \\ \theta_1 &= \theta_s \end{aligned}\right\} \text{ for } \omega_s > 0; \qquad \left.\begin{aligned} u_1 &= u_m \\ v_1 &= v_m \\ \theta_1 &= \theta_m \end{aligned}\right\} \text{ for } \omega_s \leqslant 0$$

$$D_{Mmx} = K_h \left(\frac{\partial^2 u_m}{\partial x^2} + \frac{\partial^2 u_m}{\partial y^2} \right); \quad D_{Mmy} = K_h \left(\frac{\partial^2 v_m}{\partial x^2} + \frac{\partial^2 v_m}{\partial y^2} \right)$$

$$D_{Hm} = K_h \left(\frac{\partial^2 \theta_m}{\partial x^2} + \frac{\partial^2 \theta_m}{\partial y^2} \right)$$

– equations of the t-layer:

upper surface: $h_t(x, y, t)$ impermeable
thickness: $\Delta z_t(x, y, t)$
lower surface: $h_m(x, y, t)$ permeable for entrainment fluxes only

$$\frac{\partial u_t}{\partial t} = -u_t \frac{\partial u_t}{\partial x} - v_t \frac{\partial u_t}{\partial y} - f(v_g - v_t) - c_p \theta_t \frac{\partial \pi_t}{\partial x} - g \frac{\partial h_t}{\partial x} + \frac{g \Delta z_t}{2\theta_t} \frac{\partial \theta_t}{\partial x} + \frac{\partial u_t}{\partial t}\Big|_{ent}$$

$$\frac{\partial v_t}{\partial t} = -u_t \frac{\partial v_t}{\partial x} - v_t \frac{\partial v_t}{\partial y} + f(u_g - u_t) - c_p \theta_t \frac{\partial \pi_t}{\partial y} - g \frac{\partial h_t}{\partial y} + \frac{g \Delta z_t}{2\theta_t} \frac{\partial \theta_t}{\partial y} + \frac{\partial v_t}{\partial t}\Big|_{ent}$$

$$\frac{\partial \theta_t}{\partial t} = -u_t \frac{\partial \theta_t}{\partial x} - v_t \frac{\partial \theta_t}{\partial y} + \frac{\partial \theta_t}{\partial t}\Big|_{ent}$$

$$\pi_m = \pi_t + \frac{g}{c_p \theta_t} \Delta z_t$$

$$\frac{\partial h_t}{\partial t} = \left.\frac{\partial h_m}{\partial t}\right|_{adv} - \left(\frac{\partial (u_t \Delta z_t)}{\partial x} + \frac{\partial (v_t \Delta z_t)}{\partial y} \right)$$

2.3 Turbulence Parameterization

2.3.1 Turbulent fluxes

The turbulent vertical fluxes of momentum F_M and heat F_H have to be specified at the ground h_{sur} and at the top of the surface layer h_s.

Since the model does not know vertical gradients of wind speed and temperature, a gradient parameterization of the turbulent fluxes (e.g. $F_{Mx} = K_M \partial u/\partial z$ or $F_H = K_H \partial\theta/\partial z$) is not adequate. Transfer coefficients for momentum (C_M) and heat (C_H) are used instead. Thus, the fluxes read as

– at the ground ($z = h_{sur}$):

$$F_{Mxsur} = -C_{Msur} S_{sur} u_s$$

$$F_{Mysur} = -C_{Msur} S_{sur} v_s$$

$$F_{Hsur} = -C_{Hsur} S_{sur} (\theta_s - \theta_{sur})$$

– at the interface between s-layer and m-layer ($z = h_s$):

$$F_{Mxs} = -C_{Ms} S_s (u_m - u_s)$$

$$F_{Mys} = -C_{Ms} S_s (v_m - v_s)$$

$$F_{Hs} = -C_{Hs} S_s (\theta_m - \theta_s)$$

where S denotes the 'wind shear'

$$S_{sur} = \sqrt{u_s^2 + v_s^2}$$

$$S_s = \sqrt{(u_m - u_s)^2 + (v_m - v_s)^2}$$

considering the no-slip condition $u_{sur} = v_{sur} = 0$.

The transfer coefficients at $z = h_{sur}$ (C_{Msur} and C_{Hsur}) are assumed to depend on the roughness length z_0 and on the depth of the surface layer Δz_s only. From the logarithmic wind law it follows

$$C_{Msur} = \frac{k^2}{\left[\ln\left(\frac{\Delta z_s}{z_0}\right) - 1\right]^2}$$

$$C_{Hsur} = 1.35\, C_{Msur}$$

The factor 1.35 corresponds to the inverse Prandtl number near the surface.

At the top of the surface layer $z = h_s = h_{sur} + \Delta z_s$ the magnitude of the turbulent transfer is governed by the stability:

$$C_{Ms} = \frac{k^2}{\left[\ln\left(\frac{\Delta z_s}{z_0}\right) - \psi_M(\zeta)\right]^2}$$

$$C_{Hs} = Pr(\zeta)^{-1}\, C_{Ms}$$

where ψ_M is an integrated profile function after PAULSON (1970) which reads

$$\psi_M(\zeta) = \ln\left(\frac{1+\xi^2}{2}\right) + 2\ln\left(\frac{1+\xi}{2}\right) - 2\tan^{-1}\xi + \frac{\pi}{2} \quad \text{for} \quad \zeta < 0 \quad \text{(unstable ABL)}$$

with

$$\xi = (1 - 15\zeta)^{0.25}; \quad \pi = 3.14159$$

$$\psi_M(\zeta) = 4.7\zeta \qquad \text{for} \quad \zeta > 0 \quad \text{(stable ABL)}$$

The Prandtl number is formulated after BUSINGER et al. (1971):

$$Pr = \frac{(1 - 15\zeta)^{0.25}}{1.35(1 - 9\zeta)^{0.5}} \qquad \text{for} \quad \zeta < 0$$

$$Pr = \frac{0.74 + 4.7\zeta}{1.0 + 4.7\zeta} \qquad \text{for} \quad \zeta > 0$$

The stability function ζ is expressed by the Richardson number Ri

$$\zeta = Ri \qquad \text{for} \quad Ri \leqslant 0 \text{ (unstable)}$$

$$\zeta = \frac{Ri}{1 - 4.7\,Ri} \qquad \text{for} \quad Ri > 0 \text{ (stable)}$$

where $Ri(z = h_s)$ is approximated by

$$Ri = \frac{g}{\theta_s} \frac{0.5(\Delta z_s + \Delta z_m)(\theta_m - \theta_s)}{(u_m - u_s)^2 + (v_m - v_s)^2}$$

2.3.2 Entrainment

Although the top of the ABL is material with respect to mesoscale motions, it can be changed by subgrid processes, i.e. entrainment. The rate of growth is determined following an equation introduced by DEARDORFF (1974) in the unstable case ($\theta_s > \theta_m$):

$$\left.\frac{\partial h_m}{\partial t}\right|_{ent} = 1.8\, F_{Hs} \left(\Delta z_q \frac{\partial \theta^+}{\partial z} + \frac{9\, w_*^2\, \theta_q}{g \Delta z_q}\right)^{-1} \tag{5}$$

with $\Delta z_q = h_m - h_{sur}$ (depth of the entire ABL)

$$\frac{\partial \theta^+}{\partial z} = \frac{\theta_t - \theta_m}{\Delta z_t}$$

$$\theta_q = \frac{\Delta z_s \theta_s + \Delta z_m \theta_m}{\Delta z_q}$$

$$w^* = \left(\frac{g}{\theta_q} F_{Hs}\, \Delta z_q\right)^{1/3}$$

In stable situations ($\theta_s < \theta_m$) a formula of SMEDA (1979) is used which forces the ABL to shrink after a transition from unstable to stable to an equilibrium thickness $\Delta z_q \approx 0.33\, u_*/f$ which depends only on the friction velocity u_* and the Coriolis parameter f:

$$\left.\frac{\partial h_m}{\partial t}\right|_{ent} = 0.06 \frac{u_*^2}{\Delta z_q f}\left[1 - \left(\frac{3.3\, \Delta z_q f}{u_*}\right)^3\right] \tag{6}$$

with $u_* = \sqrt{C_{Ms}}\,|V_s|$.

The combination of the entrainment Equations (5) and (6) is discussed by SMEDA and shows reasonable results for the situation of Wangara days 33/34. It should be noted that in reality the nightly ABL height is also governed by radiative cooling which cannot be considered in the dry model atmosphere. Therefore Equation (6) only gives a rough estimate of the ABL height during stable conditions.

For $(\partial h_m/\partial t)_{ent} > 0$ air of the t-layer is entrained into the m-layer which causes entrainment changes of wind speed and potential temperature in the m-layer. With $\varphi = (u, v, \theta)$ they read

$$\left.\frac{\partial \varphi_m}{\partial t}\right|_{ent} = \left.\frac{\partial h_m}{\partial t}\right|_{ent} \frac{\varphi_t - \varphi_m}{\Delta z_m} \quad \text{and} \quad \left.\frac{\partial \varphi_t}{\partial t}\right|_{ent} = 0$$

For negative values $(\partial h_m/\partial t)_{ent} < 0$ the entrainment process affects the t-layer properties:

$$\left.\frac{\partial \varphi_m}{\partial t}\right|_{ent} = 0 \quad \text{and} \quad \left.\frac{\partial \varphi_t}{\partial t}\right|_{ent} = \left.\frac{\partial h_m}{\partial t}\right|_{ent} \frac{\varphi_t - \varphi_m}{\Delta z_m}$$

2.3.3 Horizontal diffusion

The effect of horizontal diffusion induced by either wind shear or sub-grid orography is considered by the horizontal diffusion terms in the equation of motion in the s-layer and m-layer. As a result of sensitivity tests the exchange coefficient K_h was set to a constant value of $K_h = 100\ m^2 s^{-1}$.

2.4 Numerical Procedure and Initialization

The model uses forward-in-time and centered-in-space differences with the exception of the advective terms where upwind differences are applied. This combination is known to be smoothing, but it is mass consistent and saves computer time and storage. In order to fulfil the Courant criterion most efficiently the time step Δt is variable and controlled by the consideration of all signal velocities, i.e. advection and diffusion velocities, and phase velocities of gravity waves which propagate along the material surfaces.

Zero-gradient conditions are established at all lateral boundaries for all variables.

The Exner function at h_t is taken from a stable background atmosphere using the hydrostatic relation:

$$\pi_t = \pi_0 + \frac{c_p \gamma_0}{g} \ln\left(\frac{\theta_0}{\theta_0 + \gamma_0 (h_t - h_0)}\right)$$

The background atmosphere has to be prescribed by specifying the Exner function π_0 at the height h_0 and a lapse rate of the potential temperature $\gamma_0 > 0$.

The model is initialized with horizontally homogeneous distributions of the potential temperature in each model layer and spatially constant values of h_m and h_t. The initial values of the wind components within the ABL are the result of one-dimensional iterative solutions of the stationary equation of motion over each grid area. The t-layer wind is set to the geostrophic wind.

This procedure ensures a balanced initial wind field. After an integration of one to three hours the wind field is even independent of the choice of the initial value of h_m as shown by HEIMANN (1985).

3 Simulation of Wind Field Characteristics

This chapter is divided into five parts. The first one gives a general description of the application area and its typical mesoscale phenomona. A case study is discussed in the second part before we consider statistical evaluations of the model output. The simulation of one event of strong channelling will show that the model is able to reproduce this important effect. How the model was run to deduce the regional wind statistics and wind field characteristics, is explained in part 3. The following parts deal with the statistical evaluation of these runs. Frequency distributions of the wind direction (wind

roses) are presented in part 4 and compared to observations. Finally, some special characteristics of the surface wind field in the Main-Taunus region, like the diurnal variability of wind direction and channelling, are discussed in part 5.

3.1 Application of the Model to the Main-Taunus Region

Two phenomena contribute most to the regional flow statistics in orographically structured areas. These are the channelling effect, and thermally induced circulations. The channelling effect is observed even in broad valleys and along flat mountain ranges. This was pointed out by EGGER (1983) and WIPPERMANN (1984a) who also gave theoretical explanations of this phenomenon. The flow conduction even occurs in the case of neutral stratification, but it is more pronounced in stable situations. For certain directions of the geostrophic wind, the surface wind tends to show a component parallel to the valley orientation but with a sign opposite to that of the geostrophic wind. This is denoted as 'counter-current' by WIPPERMANN. His theory suggests its existence even along mountain ranges (WIPPERMANN, 1984b).

The REWIMET model is applied to the Main-Taunus region in central Germany (see Figure 2). The dominating orographical feature is the Taunus mountain range. It is orientated from southwest to northeast with an average crest altitude of 500 m above mean sea level (MSL) and has summits up to 880 m MSL (Feldberg). The mountains adjoin the Rhine-Main basin (≈ 100 m MSL).

The climate of the Main-Taunus region has been investigated during an intensive measurement campaign between 1971 and 1974 (BARTELS et al., 1976). Around 50 meteorological stations have been operating throughout the inner area in Figure 2 which is referred to as Lower-Main region ('Region Untermain') in the following.

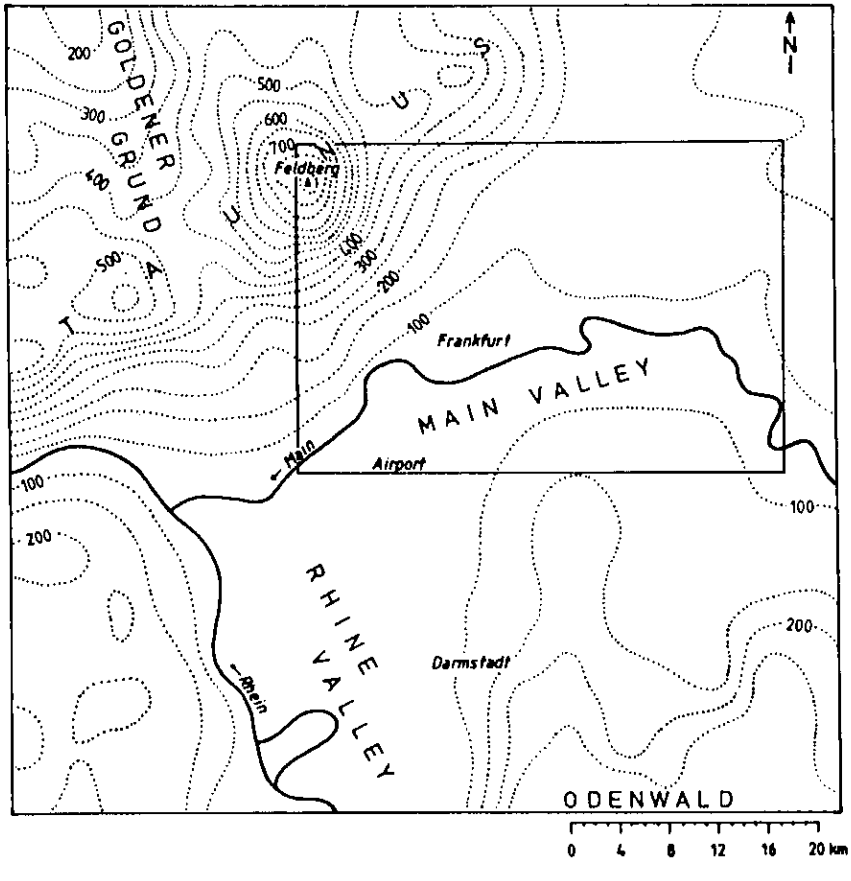

Figure 2
Map of the 'Main-Taunus region' ($68 \times 68\,km^2$). The dotted isolines represent the smoothed terrain elevation (in meters) as it is used during the model simulations. The inner frame encloses the Lower-Main region.

It was found that SSW and NNE winds prevail within a strip, roughly 20 km wide, along the Taunus mountains, although the most frequent directions of the geostrophic wind are WNW and SE. This is a consequence of the channelling effect.

Thermally generated nightly downslope winds contribute to the statistics of surface wind direction especially on the flanks of the Taunus, but their influence can be recognized even at stations on the plain close to the foot of the mountain range.

Table 1 Summary of model input parameters used in the model simulations for twelve sectors of the geostrophic winds direction.
The corresponding geostrophic wind velocities are listed in Table 2

initial values: θ_{sur} = 5.5 °C θ_s = 9.2 °C θ_m = 9.2 °C θ_t = 16.2 °C h_m = 1000 m h_t = 2000 m background atmosphere: h_0 = 2000 m θ_0 = 18.9 °C γ_0 = 4.3 K/km	grid meshes: 21 X 21 incl. boundaries 17 X 17 evaluated grid spacing: $\Delta x = \Delta y$ = 4000 m simulated time per run: τ = 3 h + 24 h (3 h precursory integration)
tendencies of θ_{sur}: − 3 ... 0 h: 0.0 K/h 0 ... 3 h: − 0.5 K/h 3 ... 6 h: 0.0 K/h 6 ... 9 h: + 1.5 K/h 9 ... 12 h: + 1.0 K/h 12 ... 15 h: + 0.5 K/h 15 ... 18 h: 0.0 K/h 18 ... 21 h: − 1.5 K/h 21 ... 24 h: − 1.0 K/h	roughness length: land use: z_0 agriculture 0.20 m forest 1.00 m suburb 1.50 m downtown 2.00 m water 0.01 m

Table 2 Annual average velocities and frequencies for all 30° sectors of the geostrophic wind in the Main-Taunus region

geostrophic wind direction sector ± 15°	annual average geostrophic speed m/s	annual frequency of occurence %
30°	5.7	4.5
60°	6.2	5.2
90°	8.2	7.8
120°	8.3	10.3
150°	8.4	8.0
180°	7.7	6.8
210°	7.6	7.2
240°	9.7	11.1
270°	10.1	14.2
300°	9.4	11.8
330°	8.1	7.4
360°	6.4	5.7

For the model runs the investigation area is resolved by a numerical grid of 17 x 17 meshes of 4 x 4 km^2 each. Two additional lateral boundary grid rows are placed for computational reasons. The topography is represented by the average elevation of each grid square and the portion of each of five types of land use (see Table 1).

3.2 A Case of Strong Channeling

A pronounced channeling occured on October 27, 1972 at 13 CET (Central European Time). A detailed analysis of the sea level pressure yields a geostrophic wind of 9.5 m/s from 170°. The vertical stratification is stable with an almost isothermal gradient throughout the lower 1000 m of the atmosphere. Figure 3 gives the distribution of the observed surface winds (≈ 10 m above ground) in the Lower-Main region. The wind direction in the eastern part of the domain corresponds to that of the geostrophic wind regarding a deflection of 20°–30° to the left caused by friction. Near Bad Homburg the flow splits. One part is diverted to the north while the other part flows almost parallel to the Taunus range towards the southwest. Since the component parallel to the mountain (orientation SW - NE) is of opposite sign compared to that of the geostrophic wind, a 'counter-current' is observed in this case.

The simulated surface layer winds of this case (Figure 4) can be compared to the observed ones within the framed area which is identical to the map sector shown in Figure 3 (Lower-Main region). However, one has to keep in mind that each calculated wind represents a surface layer grid box of 4000 x 4000 x 50 m^3, whereas the measurements are spot values taken 10 m above the ground and averaged over the period of one hour. Nevertheless apart from the wind-speeds being a little too low, the main characteristics of the flow field are simulated well enough, in particular, the stream splitting near Bad Homburg, and the northeast wind along the Taunus. Of course, some detailes do not match; for example the wind direction at Frankfurt/Airport. No 'counter-current' is simulated in the Upper-Rhine valley, but this is verified at least at Darmstadt where the synoptic station reported 3 m/s from 120° (ESE).

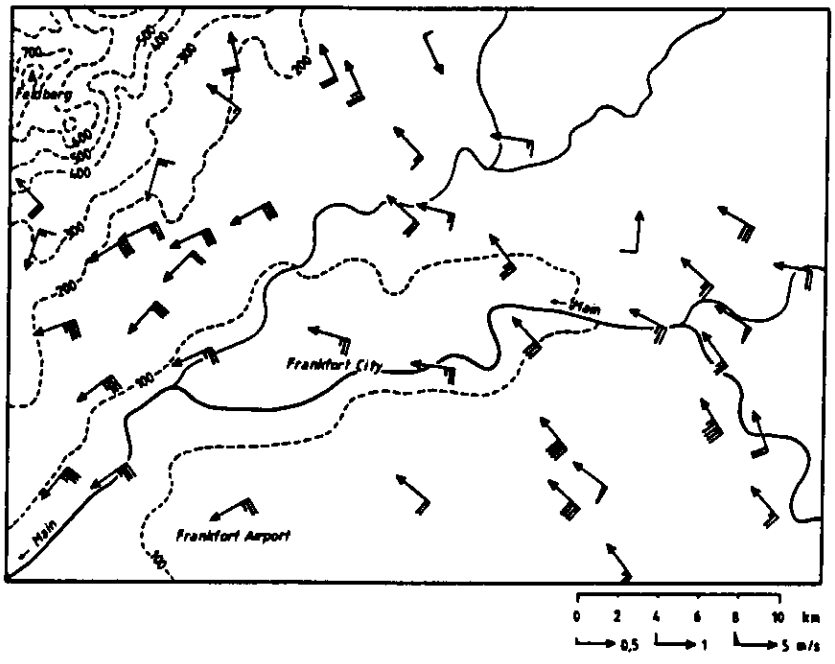

Figure 3
Measured surface wind field (≈ 10 m above ground) on October 27, 1972 13 CET in the Lower-Main region. The map sector covers the same area as the inner framed area of the maps in Figure 2 and 4.

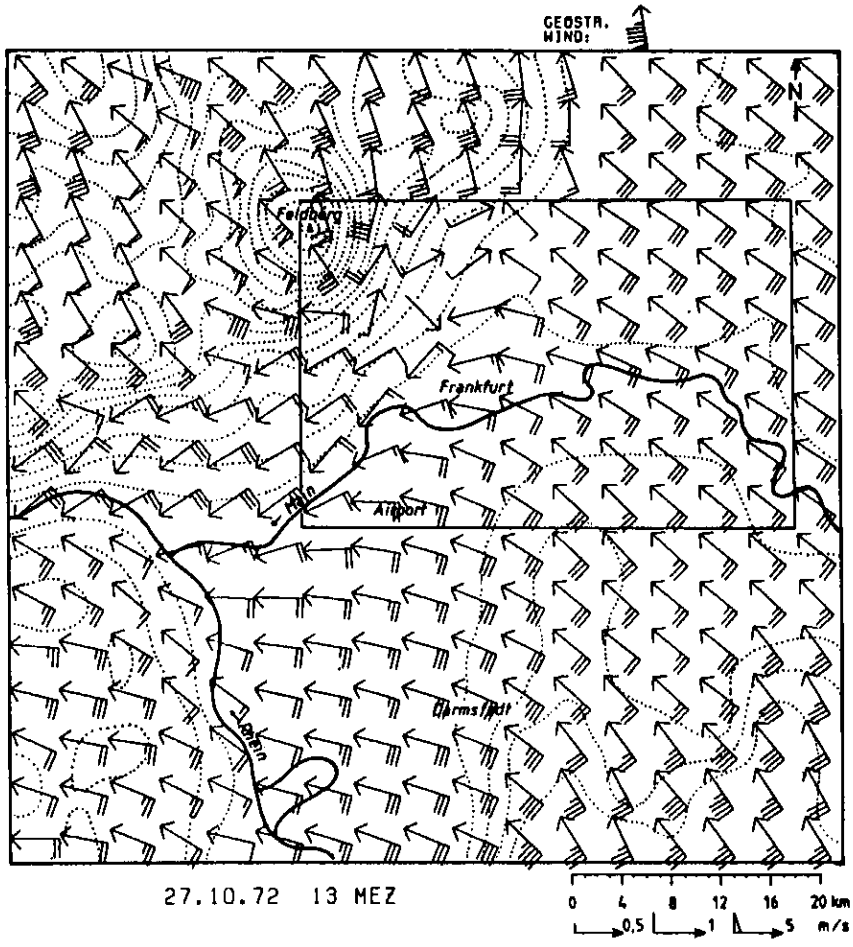

● **Figure 4**
Calculated surface layer wind field for October 27, 1972 13 CET.
The framed section (Lower-Main region) coincides with the map shown in Figure 3.

3.3 Performance of Model Runs for Regional Climate Studies

In order to gain wind roses and flow characteristics, which should represent an annual average, a set of model runs have been performed, each describing a typical diurnal cycle associated with a distinct geostrophic wind. In this way it is possible to incorporate even time-dependent processes which are connected with changing stability. In detail the following procedure was chosen:

1. The diurnal cycle

   In order to force the model thermally, the diurnal variation of the surface potential temperature θ_{sur} is prescribed identically for each run. The 3-hour tendencies of θ_{sur} are derived from the annual mean of the measured daily temperature variation at Frankfurt/Airport. The initial values of $\theta_s, \theta_m, \theta_t, h_m$, and h_t are chosen in such a way that they represent the annual average vertical stratification. For more details of the parameters see Table 1.

   The temporal progress of θ_{sur} is illustrated in Figure 5 which also indicates the response of θ_s and θ_m as it has resulted from a one-dimensional ($\partial/\partial x = \partial/\partial y = 0$) reference run.

   The change rates of θ_{sur} are reduced with increasing terrain elevation so that the amplitude of the diurnal variation in the Feldberg level (880 m MSL) is 30 % of that in the Main-Rhine plain level (100 m MSL), which again conforms to the annual average.

2. Geostrophic forcing

   Model runs of a full daily cycle (24 hours) are performed for each 30° sector of the geostrophic wind. The speed of the geostrophic wind is chosen to be the annual mean of the corresponding

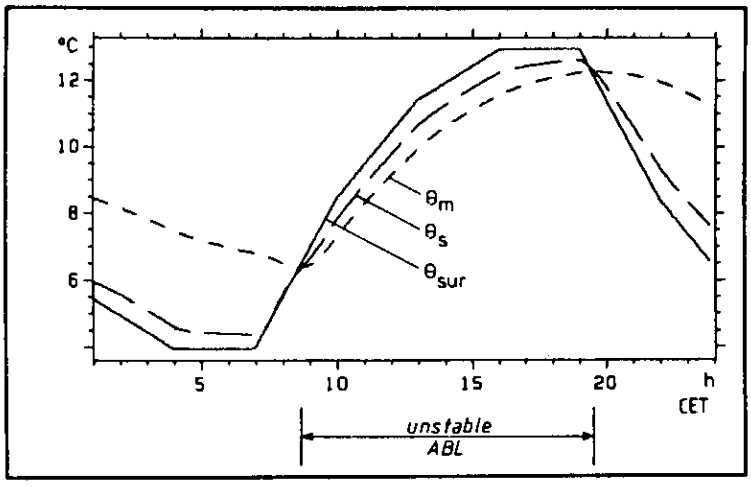

Figure 5

Simulation of the temporal variation of potential temperatures using the one-dimensional version of REWIMET.

The potential temperature at the ground Θ_{sur} was set to represent the course of a 'typical' day. Θ_s and Θ_m are the resulting potential temperatures in the s and m-layer, respectively. The atmospheric boundary layer (ABL) is unstable as long as $\Theta_s > \Theta_m$.

sector (see Table 2). These velocities were derived by averaging five years of 3 hourly values of the geostrophic wind over Frankfurt gained from the objective analysis of sea level pressure data by MANIER and DIETZER (1979).

3. Determining statistics

The frequency distribution of the 30° geostrophic wind direction sectors are also determined from the time series of the geostrophic wind at Frankfurt. See Table 2. Each model run produces 24 fields of the surface layer (s-layer) wind representing every hour of a typical day. During post-processing these fields are weighted by the frequencies of the corresponding geostrophic wind sectors. Thus, together 288 wind fields, i.e. 12 sectors x 24 hours, are available for further analysis.

3.4 Simulated Distributions of Wind Directions and Wind Speed

For the given frequency distribution of the geostrophic wind (see Table 2), two kinds of distributions of the surface layer wind have been obtained; the first by using the 1-dimensional version, i.e. simulating homogeneous topography ($\partial/\partial x = \partial/\partial y = 0$), and the second by applying the 3-dimensional version, i.e. considering the real inhomogeneous topography.

The frequency distribution for homogeneous terrain is added to all the graphs of Figure 6 in order to demonstrate the capability of 3-dimensional simulations that include the full topographic information. The best agreement between observed and simulated frequency distributions (inhomogeneous topography) is found at Frankfurt/Airport (Figure 6a). Although not all peaks match at the other stations, some characteristic features of the frequency distributions are sufficiently reproduced, e.g. the high probability of northwest winds on the Feldberg (Figure 6c).

Figure 7 shows all calculated surface layer wind roses within the Main-Taunus region. Around Frankfurt/Airport, for example, the 210° and 240° sectors are favoured as well as the 30° and 60° ones. The most frequent directions are almost parallel to the Taunus range which is a consequence of the channeling effect. The remarkable SSW-NNE orientation of the wind roses occurs mainly in the Lower-Main valley within a strip parallel to the Taunus crest line. Other areas which also show a well pronounced channeled flow are the Rhine valley near Wiesbaden, and the SSE-NNW orientated valley named 'Goldener Grund' in the northwestern most part of the investigation area. But a weak channeling effect is evident even in the Upper-Rhine valley between Darmstadt and the southern boundary of the grid domain. In other parts of the region the wind direction frequencies are distributed more uniformly as in the northeast.

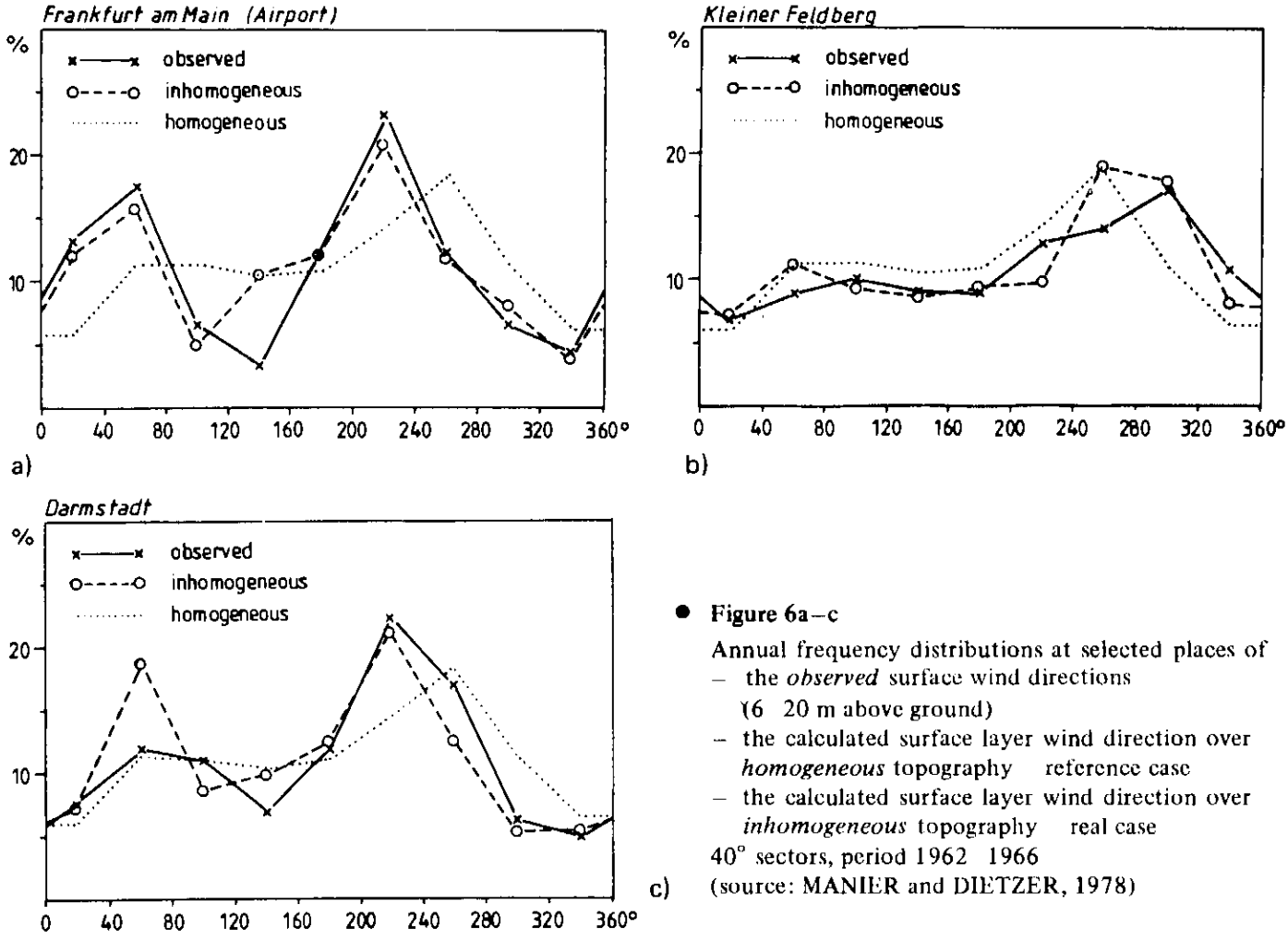

● **Figure 6a–c**

Annual frequency distributions at selected places of
- the *observed* surface wind directions
  (6 20 m above ground)
- the calculated surface layer wind direction over *homogeneous* topography reference case
- the calculated surface layer wind direction over *inhomogeneous* topography real case

40° sectors, period 1962 1966
(source: MANIER and DIETZER, 1978)

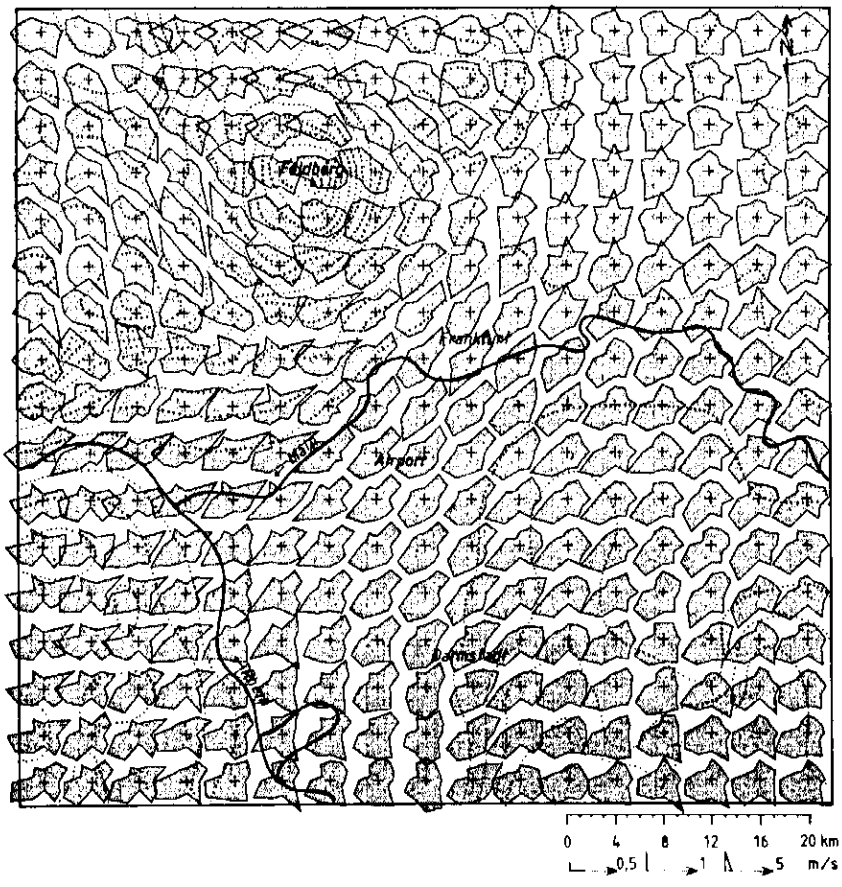

● **Figure 7**

Field of synthetic annual wind roses (30° sectors) of the surface layer winds gained by evaluating 288 model runs using the three-dimensional version of REWIMET (real inhomogeneous topography of the Main-Taunus region).

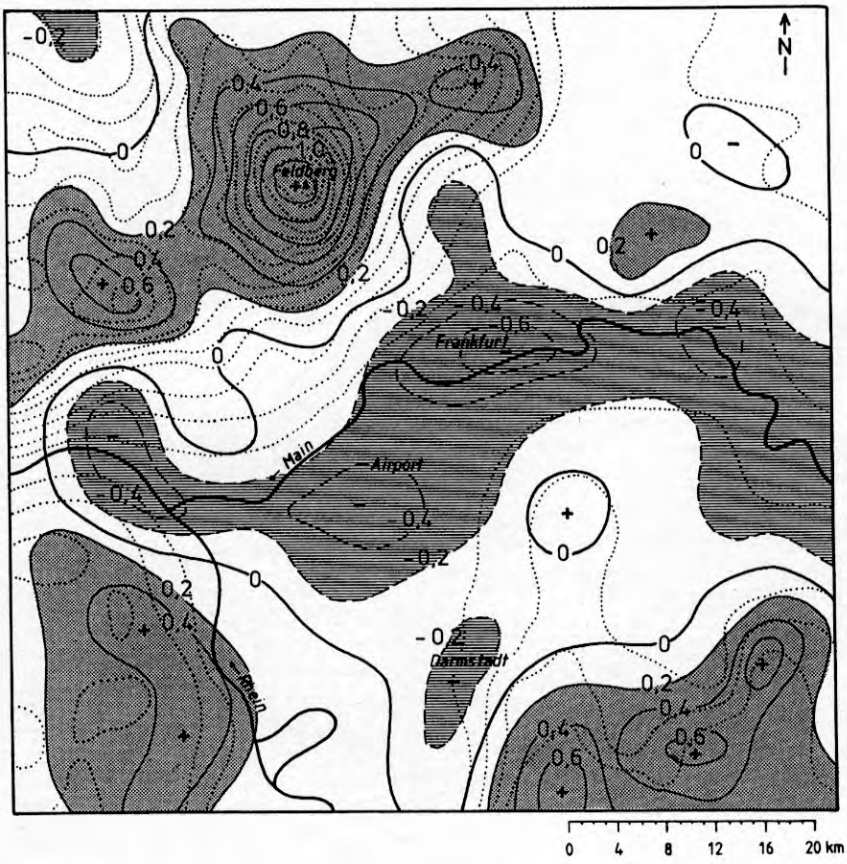

● **Figure 8**
Calculated average surface layer velocity deviation (m/s) of the real case (*inhomogeneous* topography) from the reference case (*homogeneous* topography).

As the wind direction is influenced by the topography, so is the wind speed. Figure 8 illustrates the spatial distribution of the average surface layer wind velocity difference between the inhomogeneous real case and the homogeneous reference case. The wind speed is reduced by the topography over the plains (by 0.4 m/s over Frankfurt/Airport, for example) and especially over the rougher cities (Wiesbaden, Frankfurt, Hanau). In contrast, the velocities are increased over elevated terrain with a maximum on the Feldberg where the wind is speeded up by 1.2 m/s on average. The simulated spatial average wind speed distribution is confirmed by the observations which give a mean annual velocity difference of 1.8 m/s between Frankfurt/Airport and Feldberg.

3.5 Wind Field Characteristics

The discussion will now be focused on the following questions which often arise in association with regional planning and environmental studies:

- Were do daily circulation systems tend to occur?
- Where do distinct sectors of the geostrophic wind frequently cause channeling, and where does the flow split?

The effect of thermally circulating systems is measured by the ratio R of the vector mean to the scalar mean of the surface layer wind averaged over a daily cycle (24 hours).

$$R(x, y) = 100\,\% \cdot \frac{\left| \sum_{t=1}^{24} \mathbf{V}_s\,(x, y, t) \right|}{\sum_{t=1}^{24} |\mathbf{V}_s(x, y, t)|}$$

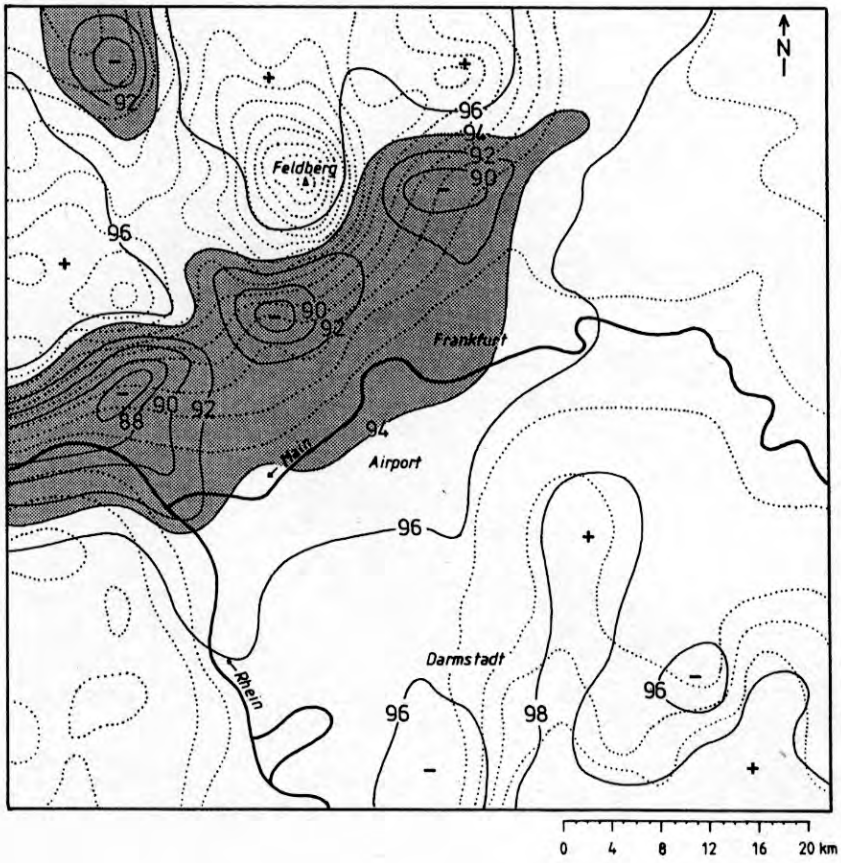

● **Figure 9**
Persistency of direction indicated by the ratio of the vector mean to the scalar mean of the calculated surface layer winds (real case) during the course of a 'typical' day averaged over all twelve 30°-sectors of the geostrophic wind.

R, expressed in percent, is a measure of the temporal persistency of wind direction. It is close to 100 %, if the wind direction does not vary much during the day, and it becomes rather small in the case of strongly developed thermal circulation with winds shifting between day and night. The distribution of a mean R, averaged over the twelve different directions of $\mathbf{V}_g$, is shown in Figure 9. Since the surface layer wind direction also varies due to changing stability the constancy of direction does not reach 100 % within the Main-Taunus region, but it is rather high ($\approx$ 98 %) over ridges (e.g. the Odenwald) and summits (e.g. the Feldberg). The main slope wind regimes are found over the south-eastern flank of the Taunus, and in the SE-NW orientated 'Goldener Grund' valley. Since the strength of channeling also depends on the diurnal variation of stability, a reduced persistency of the surface layer wind direction is detected even over parts of the Main-Rhine plain, and in the Upper-Rhine valley south of Darmstadt.

For many applications of mesoscale models it is worth knowing about the sensitivity of the locally calculated wind direction to variations of the large scale geostrophic wind direction. Then, for instance, it is possible to estimate the required accuracy of the prescribed geostrophic wind, and to identify typical trajectories along which pollutants are transported for a wide range of geostrophic wind directions. Therefore, the model runs have been evaluated also for distinct sectors of the geostrophic wind. They were chosen so that the Taunus could be expected to have a marked effect.

Figure 10 shows the mean vectors of the surface layer wind for the geostrophic directions 30°, 60°, ... ,150°, again weighted by the probability of their annual occurence. The channeling along the Taunus range is well pronounced, but a diversion to the south in the Upper-Rhine valley can also be recognized. As a measure of the persistency of the surface layer wind direction in respect to variations in the geostrophic wind direction we again use the ratio of the vector mean to the scalar mean. In the dotted area the persistency of the surface layer wind exceeds the corresponding value of the geostrophic

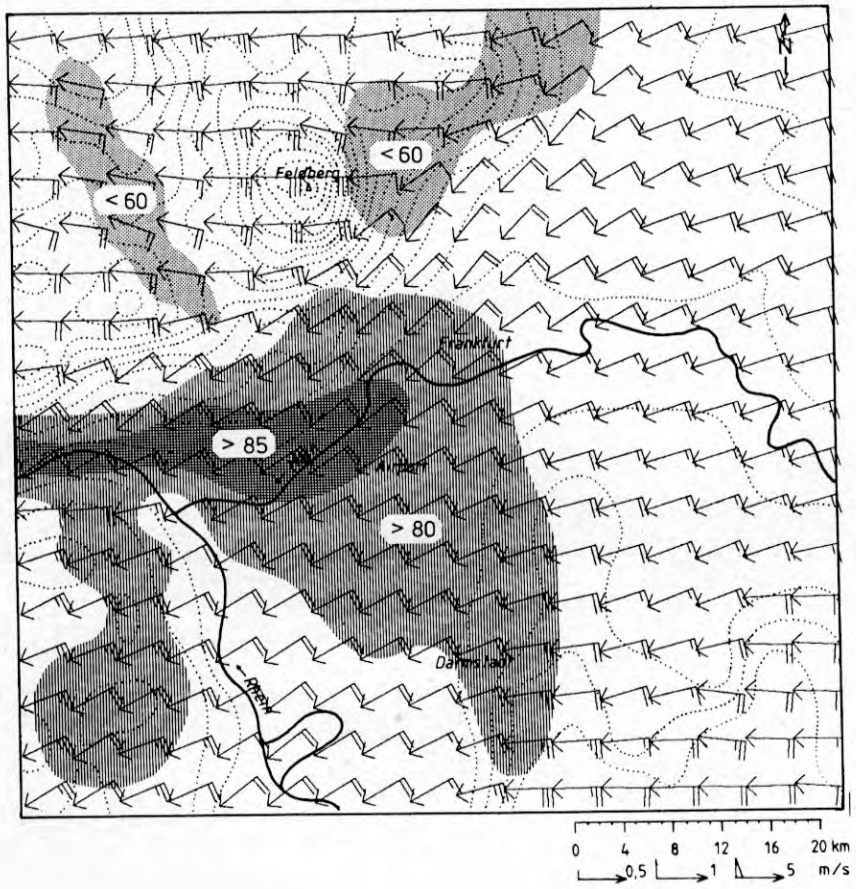

● **Figure 10**
Vector mean of the calculated surface layer winds (real case) averaged over the 24 hour variations of the geostrophic directions 30°, 60°, ..., 150°. The shaded areas indicate the persistency of the calculated surface layer wind direction during the prescribed variation of Θ_{sur} and V_g (see text).

wind (80 %). This means that channeling is specially likely along the Main river west of Frankfurt for geostrophic winds from 30° to 150°. The field of the mean surface layer wind vectors indicates a flow splitting in the north-eastern part of the Taunus. In this area the wind direction is highly sensitive to these variations of the geostrophic direction.

4 Conclusions

The hydrostatic three-layer model REWIMET is used for the numerical synthesis of regional (i.e. mesoscale-β) surface layer wind field characteristics induced by gentle topography. Steep orography and local (mesoscale-γ) effects cannot be treated with this model. Time dependent processes which are due to changing stability were incorporated by computing full daily cycles and evaluating 24 wind fields during the course of a typical day. Twelve such runs were performed covering all 30° sectors of the geostrophic wind. They were weighted with the corresponding annual probability of occurence for further evaluation.

Of course, this set of 288 wind fields hardly represents the full variability of one year. Seasonal effects and different amplitudes of the daily surface temperature variation have not been considered so far. Instead of distinguishing several classes of geostrophic wind speed, the annual mean speed of each 30° sector was prescribed during this study.

Nevertheless, the simulated annual distributions of the surface layer wind reproduce the observations quite well. This makes it possible to apply the model to various problems of regional climate and air quality studies. Different wind regimes can be identified and their frequency can be estimated. The procedure also allows wind monitoring stations to be assessed for spatial representativeness.

Further statistical evaluations can be made on other model parameters like the atmospheric boundary layer height, for instance. Moreover, it is possible to invoke the transport equation in order to extend the method to air pollution dispersal problems. The model then allows the mean regional concentration patterns to be estimated and source-receptor relations to be studied.

References

BARTELS, H., RUDOLF, B., SWANTES, H. J. and VENT-SCHMIDT, V., 1976: Klima als Faktor der Regionalplanung. In: Lufthygienisch-meteorologische Modelluntersuchung in der Region Untermain, Regionale Planungsgemeinschaft Untermain, Frankfurt a.M.

BUSINGER, J. A., WYNGAARD, J. C., IZUMI, J. C. and BRADLEY, F., 1971: Flux-Profile Relationships in the Atmospheric Surface Layer. J. Atmos. Sci. **28**, 181–189.

DEARDORFF, J. W., 1972: Parameterization of the Planetary Boundary Layer for the Use in General Circulation Models. Mon. Wea. Rev. **100**, 93–106.

DEARDORFF, J. W., 1974: Three-Dimensional Numerical Study of the Height and Mean Structure of the Heated Planetary Boundary Layer. Bound. Lay. Meteor. 7, 81–106.

DEARDORFF, J. W., UEYOSHI, K. and HAN, Y.-J., 1984: Numerical Study of Terrain-Induced Mesoscale Motions and Hydrostatic Form Drag in a Heated, Growing Mixed Layer. J. Atmos. Sci. 41, 1420–1441.

EGGER, J., 1983: Kanalisierung des Windes in breiten Tälern. Ann. Meteor. **20**, 8–10.

GROSS, G., 1985: An Explanation of the "Maloja-serpent" by Numerical Simulation. Beitr. Phys. Atmosph. **58**, 441–457.

HAN, Y.-J., UEYOSHI, K. and DEARDORFF, J. W., 1982: Numerical Study of Terrain-Induced Mesoscale Motion in a Mixed Layer. J. Atmos. Sci. **39**, 2464–2476.

HEIMANN, D., 1985: Ein Dreischichten-Modell zur Berechnung mesoskaliger Wind- und Immissionsfelder über komplexem Gelände. Dissertation Fak. f. Physik, Universität München.

KEYSER, D. and ANTHES, R. A., 1977: The Applicability of a Mixed-Layer Model of the Planetary Boundary Layer to Real-Data Forecasting. Mon. Wea. Rev. **105**, 1351–1371.

LAVOIE, R. L., 1972: A Mesoscale Numerical Model of Lake-Effect Storms. J. Atmos. Sci. **29**, 1025–1040.

MANIER, G. and DIETZER, B., 1979: Untersuchung über den Einfluß der Topographie der Erdoberfläche auf den Zusammenhang zwischen den Häufigkeitsverteilungen von Bodenwind und geostrophischem Wind. Meteorol. Rdsch. **32**, 35–44.

PAULSON, C. A., 1970: The Mathematical Representation of Wind Speed and Temperature Profiles in the Unstable Atmospheric Surface Layer. J. Appl. Meteor. 9, 857–861.

SMEDA, M. S., 1979: Incorporation of Planetary Boundary Layer Processes into Numerical Boundary Layer Models. Bound. Lay. Meteor. 16, 115–129.

VAN EGMOND, N. D. and KESSEBOOM, H., 1983: Mesoscale Air Pollution Dispersion Models-I. Eulerian Grid Model. Atmos. Environ. **17**, 257–274.

WIPPERMANN, F. and GROSS, G., 1981: On the Construction of Orographically Influenced Wind Roses for Given Distributions of the Large-Scale Wind. Beitr. Phys. Atmosph. 54, 492–501.

WIPPERMANN, F., 1984a: Air Flow over and in Broad Valleys: Channeling and Counter-Current. Beitr. Phys. Atmosph. 57, 92–105.

WIPPERMANN, F., 1984b: Do Flat Mountain Ranges also Channel the Air Flow? Beitr. Phys. Atmosph. 57, 282–284.